Lab on a Chip

Accepted Manuscript

ROYAL SOCIETY OF CHEMISTRY

www.rsc.org/loc

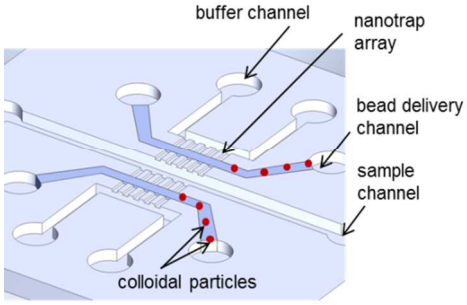

We have applied a simple evaporation based self-assembly technique to create a sub-50nm nanofluidic junction between two microchannels in PDMS.

Journal Name

RSCPublishing

TECHNICAL INNOVATION

Creating Sub-50 nm Nanofluidic Junctions in PDMS Microchip via Self-Assembly Process of Colloidal Silica Beads for Electrokinetic Concentration of Biomolecules

Cite this: DOI: 10.1039/xoxxoooooox

Received ooth January 2012,
Accepted ooth January 2012

DOI: 10.1039/xoxxoooooox

www.rsc.org/

A. Syed,[a] L. Mangano,[b] P. Mao,[b] J. Han[b,c] and Y.-A. Song[a,d]*

In this work we describe a novel and simple self-assembly of colloidal silica beads to create nanofluidic junction between two microchannels. The nanoporous membrane was used to induce ion concentration polarization inside the microchannel and this electrokinetic preconcentration system allowed rapid concentration of DNA samples by ~1700 times and protein samples by ~100 times within 5 minutes.

Introduction

The emerging field of the nanofluidics allows unprecedented possibility to manipulate transport of ions and biomolecules. Especially around the length scale of $10^1 - 10^2$ nm, where a transition from single molecules to bulk phase takes place, there are several new phenomena observed, which offer unique opportunities to study chemical operations such as concentration and ion selection.[1, 2] The nanoscale channel size combined with the surface charge enables a size- and charge-based separation of biomolecules and ions. A common device platform for the study of nanofluidics is a two-microchannel system connected by an array of nanochannels as a nanoscale junction.[3-5]

As for the choice of materials, the most commonly used materials are silicon and glass due to their well-developed fabrication technique and the stiffness of the materials allowing channels down to a few tens of nanometers without collapsing;[6] however, fabrication of nanochannels in silicon and glass using photolithography and wet etching is costly and time-consuming.[7-9] Alternatively, less expensive material such as poly(dimethylsiloxane) (PDMS) is gaining more popularity in nanofluidics. It offers several advantages over silicon and glass in terms of fabrication such as moldability for easy, rapid replication and convenient bonding. However, due to the flexibility of the material with a Young's modulus of 360-870 KPa, nanochannels in such soft substrate are prone to collapse and deform. As an alternative to the soft lithography route, several non-lithographic methods have also been developed to fabricate nanochannels directly in PDMS without casting against molds with nanopatterns. In the first method, plasma-oxidized PDMS was stretched to produce cracks with mean depth of 78 nm.[10] The size of these cracks, and therefore that of the nanochannels can be reversibly altered by applying pressure. However, precise control of the nanochannel size by applying pressure remains a challenge considering the variability of the PDMS layer thickness and stiffness. In a later study, PDMS was stretched under oxygen plasma to form wrinkles whose amplitude and wavelength could be controlled by exposure time and strain.[11] A channel collapse method allows more complex geometry for nanochannels with dimensions as low as 60 nm.[12] Even though these non-lithographic approaches allow fabricating nanochannels below 100 nm depth, all these approaches are still limited in the controllability of nanochannel sizes, as well as in the ability to perform surface functionalization of the nanochannels of the device both of which are critically important in most nanofluidic devices. Previously, colloidal crystal self-assembly induced by evaporation,[13-15] electrocapillary forces,[16, 17] and centrifugal force[18] has been reported for microfluidic devices.

To create a nanofluidic junction between two microchannels in a controlled way with a facile surface functionalization, we have deployed a self-assembly process of colloidal silica beads in a microchannel driven by evaporation. Colloidal crystals have received attention for applications in photonics, yet they hold promise as nanoporous membranes as well. Colloidal crystal growth is induced by evaporation and the resulting close-packed structure has pores with diameters ~15% of the colloidal particle diameter.[13] In addition to the pore size controllability, it has been demonstrated that surface properties of colloidal particles can easily be modified via layer-by-layer self-assembly of polyelectrolytes.[19] Once self-assembled in the microchannel, the size of the colloidal particles coated with polyelectrolytes, and therefore the size of the pores, could be further tuned by temperature,[20] pH,[21, 22] and ionic strength.[21] Recent biological applications of colloidal silica to microfluidics are electrochromatography,[23] biosensors,[24] and separation of proteins and DNA.[13, 25]

In order to demonstrate a proof of concept for our approach, we built an electrokinetic preconcentration device in PDMS (detailed fabrication and assembly in supplementary information) that requires a nanoporous cation-selective membrane as a junction between two microfluidic channels.

Results and discussion

Colloidal self-assembly

Electrokinetic trapping uses ion-selective membranes to create a depletion region which traps charged molecules when coupled with a tangential electrokinetic flow inside a microfluidic channel, allowing them to become concentrated. Generally, such devices require nanoscale features in the membrane on the order of the EDL (electrical double layer) thickness, which cannot be reproduced reliably using PDMS/soft lithography. Instead, microfluidic devices with silicon nanochannels have been used to initiate ion depletion and preconcentration.[4] A photographic image of such a concentration device in PDMS is shown in Figure 1a. The sample delivery channel in the middle is connected to the buffer solution channel on each side via a 50 μm wide colloidal bead delivery channel (Figure 1b). It is used for filling the silica bead suspension and thus creating a nanoporous junction between the sample and the buffer channel (Figure 1c).

Figure 1. Microfluidic concentrator in PDMS with integrated sub-50 nm nanofluidic junctions, a) photo of the concentrator device. b) Schematic of the micro-nanofluidic device with a bead delivery channel between the main and buffer channel. The voltage is applied across the nanoporous membrane between the sample channel and the buffer channels. c) Micrograph of the device with a colloidal particle assembly inside the upper and lower bead delivery channels. View A: SEM of self-assembled 300 nm silica colloidal particles trapped with the nanotrap arrays between the sample and buffer channel (for higher magnification picture see Figure S1 in SI).

To trap the colloidal particles in the delivery channel while maintaining a fluidic connection between the sample and buffer channel, an array of lithographically patterned nanochannels with a depth of 700 nm and a width of 2 μm was used on both sides of the filling channel (Figure 1c, view A, see the fabrication method in Experimental section). The aspect ratio of width to depth was below the limit of 10:1. Using the capillary force inside the temporarily hydrophilic microchannel immediately after plasma bonding, the silica bead suspension was flown into the 10 μm deep delivery channel and the suspended beads got trapped at the end of the delivery channel where the reservoir hole interfaces with the microchannel. The lithographically patterned nanochannels prevented the particles from entering into the sample or side buffer channels. The air-liquid meniscus is pinned at the entrance of the nanochannel and the surface tension required to prevent bead suspension from passing through the nanochannel can be estimated as follows:[26]

$$\Delta P_{LP} = \frac{4\gamma\cos\theta}{d} \approx 193 \text{ kPa}, \quad (1)$$

Where γ is the surface tension between gas and water (~72 mN/m), θ is the contact angle (46 ° for plasma-treated PDMS surface for 100 s),[27] d is the diameter of a circular cross section (in our case we assumed a hydraulic diameter D_H =2wh/(w+h)=2 x 2 μm x 700 nm/(2 μm + 700 nm) = 1.037 μm for each rectangular cross sectional nanochannel with a width w and height h).

As a result, the continuously supplied silica beads self-assemble to form a homogeneous nanostructure inside the bead delivery channels. With the help of these traps, we could trap silica beads from a diameter of 900 nm down to 300 nm, as shown in Figure 1c, view A. A topographical characterization of the traps before plasma bonding to a glass substrate can be found in Figure S3 of supporting information. Since the pore size of the 300, 500 and 900 nm silica bead assembly was estimated to be ~60, 90 and 170 nm respectively (~18% of the particle diameter, Figure S4, in SI), approximately in the range of the electrical double layer thickness, an overlapped EDL was expected to induce an ion selectivity of the silica colloidal membrane.

Electrokinetic preconcentration

To validate the ion-selectivity of the silica bead assembly, we applied potential difference across the 300 nm colloidal membrane and observed an ion depletion region near the nanofluidic junction, as the time-lapse images show in Figure 2. This ICP (ion concentration polarization) phenomenon is characteristic for the cation-selective membranes due to a preferred transport of the cations through the cation-selective membrane. The fact that we observed a formation of the ion depletion region implied that the pore size of the silica bead array was on the order of EDL thickness. The thickness of the electrical double layer is approximately that of the Debye screening length $\lambda_{D:}$

$$\lambda_D = \sqrt{\varepsilon\varepsilon_0 k_B T / 2 n_{bulk} z^2 e^2} \quad (2)$$

(ε: dielectric constant of water, $\varepsilon_{0:}$ permittivity of vacuum, k_B: Boltzman constant, T: absolute temperature, n_{bulk}:bulk ion concentration (M), z: valency of the ions, e: charge of an electron).

Under most actual ionic conditions, λ_D is between 1 and 10 nm. Previously, we observed a similar result with the lithographically patterned nanochannels with a channel depth of 40 nm in a silicon microchip.[4]

The electrokinetic preconcentration system described here allowed rapid concentration of biomolecules. 10 nM Cy5 tagged DNA (CAA CCG ATG CCA CAT CAT TAG CTA C) in 1 mM PB (phosphate buffer) was used for preconcentration. For 300 nm and 500 nm silica beads, 30 V (20.66 $V.cm^{-1}$, the

distance between two electrodes was 1.45 cm) was applied across the sample channel to initiate ion depletion region formation. By applying an electroosmotic flow in the tangential direction with a voltage difference of V_2-V_1 =1 V (0.69 V.cm^{-1}) for 300 nm silica beads and V_2-V_1 =5 V (3.44 V.cm^{-1}) for 500 nm silica beads, we could increase the concentration of the DNA sample by ~1700 folds in 15 minutes (Figure 3a, b, VideoS1 in SI). As shown in Figure 3b, 500 nm beads allowed more robust concentration performance across devices than 300 nm beads. The plug was initiated near the colloidal nanofluidic junctions and was stable even after 15 minutes.

Figure 2. Time-lapse micrographs show the formation of an ion depletion region near the nanofluidic colloidal junctions in the channel filled with DNA (initial concentration of 10 nM). The ion depletion region was initiated at t=10 s and a concentrated DNA plug was generated at V_2 = 30V and V_1 = 25V across the sample channel while the buffer channels were grounded. The dotted lines have been used to highlight the channels walls. A concentration factor of ~1700 folds was achieved within 15 minutes using 300 nm colliodal membrane.

To study the effect of surface functionalization on the charge selectivity of the pores and thus on the concentration performance, we used 500 nm silica amine particles coated with a single layer of PSS and 500 nm silica carboxyl particles coated with a layer of PAH and PSS (Figure 3 c and d). Although lower voltages (8 V (5.51 V.cm^{-1}) and 10 V (6.89 V.cm^{-1}) for silica amine/PSS and silica carboxyl/PAH/PSS beads respectively) were applied to initiate ion depletion region, the concentration factor achieved was not higher than that of bare silica beads. The amine/PSS-coated beads showed ~200-fold increase in DNA concentration at a voltage difference of 1 V after 15 minutes (Figure 3c) and the carboxyl/PAH/PSS bead membrane showed a 1000-fold increase at a voltage difference of 2 V (1.38 V.cm^{-1}) after 15 minutes (Figure 3d). In both cases, the concentration data showed a significant standard deviation between devices which seems to suggest that an adjustment of the device layout is necessary depending on the increased amount of zeta potential through surface functionalization. Applying higher voltage (30V) to initiate ICP led to an increase in the concentration of DNA plug but it also made the plug unstable (Video S2 in SI). V_1 had to be continuously tuned to keep the plug near the membrane. This phenomenon can be attributed to strong ion depletion region formation caused by higher surface charge of the polyelectrolyte-coated beads which repelled the concentration plug farther away from the membrane junction and resulted in less stable concentration behavior. Also, the bead delivery channel parallel to the sample channel acted as a long membrane (~1 mm), often creating multiple ion depletion regions in the sample channel due to insufficient thickness of the PDMS wall of 25 μm between the bead delivery and the sample channel (Video S3 in SI). This can be overcome in future by reducing the width as well as the length of the bead delivery channel so that the colloidal membrane forms only a narrowly confined nanofluidic junction between the sample and buffer channel, preferably at ~100 μm.

Figure 3. Average fluorescence intensity of DNA as a function of time with a nanoporous membrane of (a) 300 nm silica beads (b) 500 nm silica beads and (c) 500 nm silica amine beads coated with a single layer of PSS and (d) 500 nm silica carboxyl beads coated with two layers of PAH and PSS. The dotted lines represent the signal level for 10 nM (a,b,c,d), 17 μM (a, b), 2 μM (c) and 10 μM (d) DNA. The concentrated plug was generated at (a) V_2=30, V_1=29, (b) V_2=30, V_1=25, (c) V_2=8, V_1=7 and (d) V_2=10, V_1=8 volts. Each set of data points represents an independent experiment. The results have been normalized against background fluorescence.

In addition to DNA, 4 μg mL^{-1} of fluorescent protein BPE (B-Phycoerythrin, Figure S5, in SI) in 1 mM PBS (phosphate buffered saline) was also used to validate the system. Using the ion-selective colloidal membrane, we could increase the concentration of BPE by ~100 times within 5 minutes.

Conclusions

We have applied a simple self-assembly technique to create a sub-50nm nanofluidic junction between two microchannels in PDMS. Even though PDMS offers several key advantages such as easy moldability and simple bonding technique, it is very challenging to fabricate sub-50nm junction in PDMS due to the softness of the material. However, by using the self-assembly process of the colloidal silica beads, we were able to create a sub-50 nm nanofluidic junction in a PDMS microchannel. Using the self-assembled colloidal silica membrane with an estimated pore size of ~45 nm, we could demonstrate an ion concentration polarization near the nanofluidic junction and concentrate a DNA sample by ~1700 times and protein sample by ~100 times. With this approach, we can easily adjust the pore size for ionic and molecular transport through the membrane simply by varying the bead size. Compared to the silicon-based nanochannels, the major advantage of the self-assembled colloidal membrane is the possibility of performing the surface functionalization completely outside the sealed microfluidic device in a separate vial. We believe that this approach opens up a possibility to fabricate a micro/nanofluidic platform rapidly with easily tunable pore sizes either by controlling the bead size, ionic strength or the pH value of the buffer solution for the study of ionic and molecular transport in 10-100 nm regime.

Acknowledgements

This work was supported by NIH R21 EB008177-01A2. We thank the staff of MIT Microsystems Technology Laboratory for the support during fabrication and James Weston and Nikolas Giakoumidis of NYUAD for SEM pictures and custom made voltage divider respectively.

Notes and references

[a] New York University Abu Dhabi, Division of Engineering, PO Box 129188, Abu Dhabi, UAE.
[b] Department of Electrical Engineering and Computer Science, Massachusetts Institute of Technology, Cambridge, MA 02139, USA.
[c] Department of Biological Engineering, Massachusetts Institute of Technology, Cambridge, MA 02139, USA.
[d] Department of Chemical and Biomolecular Engineering, New York University Polytechnic School of Engineering, Brooklyn, NY 11201, USA.
[*] E-mail: rafael.song@nyu.edu

Electronic Supplementary Information (ESI) available: [Experimental details and additional information included in ESI]. See DOI: 10.1039/b000000x/

1. K. Mawatari, Y. Kazoe, H. Shimizu, Y. Pihosh, T. Kitamori, *Anal Chem*, 2014, **86**, 4068-4077.
2. T. Tsukahara, K. Mawatari, T. Kitamori, *Chem. Soc. Rev.*, 2010, **39**, 1000-1013.
3. K. Aizel, V. Agache, C. Pudda, F. Bottausci, C. Fraisseix, J. Bruniaux, F. Navarro, Y. Fouillet, *Lab Chip*, 2013, **13**, 4476-4485.
4. Y. C. Wang, A. L. Stevens, J. Han, *Anal Chem*, 2005, **77**, 4293-4299.
5. R. Karnik, R. Fan, M. Yue, D. Li, P. Yang, A. Majumdar, *Nano letters*, 2005, **5**, 943-948.
6. P. Mao, J. Y. Han, *Lab Chip*, 2005, **5**, 837-844.
7. P. Mao, J. Han, *Lab Chip*, 2009, **9**, 586-591.
8. A. Balducci, P. Mao, J. Y. Han, P. S. Doyle, *Macromolecules*, 2006, **39**, 6273-6281.
9. M. Yamada, P. Mao, J. P. Fu, J. Y. Han, *Anal Chem*, 2009, **81**, 7067-7074.
10. D. Huh, K. L. Mills, X. Y. Zhu, M. A. Burns, M. D. Thouless, S. Takayama, *Nat Mater*, 2007, **6**, 424-428.
11. S. Chung, J. H. Lee, M. W. Moon, J. Han, R. D. Kamm, *Adv Mater,* 2008, **20**, 3011-3016.
12. S. M. Park, Y. S. Huh, H. G. Craighead, D. Erickson, *Proc. Natl. Acad. Sci*., 2009, **106**, 15549-15554.
13. Y. Zeng, D. J. Harrison, *Anal Chem*, **2007**, 79, 2289-2295.
14. A. Malekpourkoupaei, L. W. Kostiuk, D. J. Harrison, *Chemistry of Materials,* 2013, **25**, 3808-3815.
15. A. Merlin, J.-B. Salmon, J. Leng, *Soft Matter*, 2012, **8**, 3526-3537.
16. J.-Y. Shiu, C.-W. Kuo, P. Chen, *Journal of the American Chemical Society*, 2004, **126**, 8096-8097.
17. J. Y. Shiu, P. Chen, *Adv Mater*, 2005, **17**, 1866-1869.
18. S.-K. Lee, G.-R. Yi, S.-M. Yang, *Lab Chip*, 2006, **6**, 1171-1177.
19. G. B. Sukhorukov, E. Donath, H. Lichtenfeld, E. Knippel, M. Knippel, A. Budde, H. Mohwald, *Colloid Surface A*, 1998, **137**, 253-266.
20. O. Schepelina, I. Zharov, *Langmuir*, 2007, **23**, 12704-12709.
21. O. Schepelina, I. Zharov, *Langmuir*, 2008, **24**, 14188-14194.
22. J. J. Smith, I. Zharov, *Langmuir*, 2008, **24**, 2650-2654.
23. A. Gaspar, L. Hernandez, S. Stevens, F. A. Gomez, *Electrophoresis*, 2008, **29**, 1638-1642.
24. S. Y. Lee, S. H. Kim, S. G. Jang, C. J. Heo, J. W. Shim, S. M. Yang, *Anal Chem*, 2011, **83**, 9174-9180.
25. D.-W. Zhang, H.-Q. Zhang, L. Tian, L. Wang, F. Fang, K. Liu, Z.-Y. Wu, *Microfluid Nanofluid*, 2013, **14**, 69-76.
26. P.-G. de Gennes, F. Brochard-Wyart, D. Quere, Capillarity and wetting phenomena: drops, bubbles, pearls, waves, Springer, New York, 2004.
27. S. H. Tan, N. T. Nguyen, Y. C. Chua, T. G. Kang, *Biomicrofluidics*, 2010, **4**.

Journal Name RSCPublishing

TECHNICAL INNOVATION

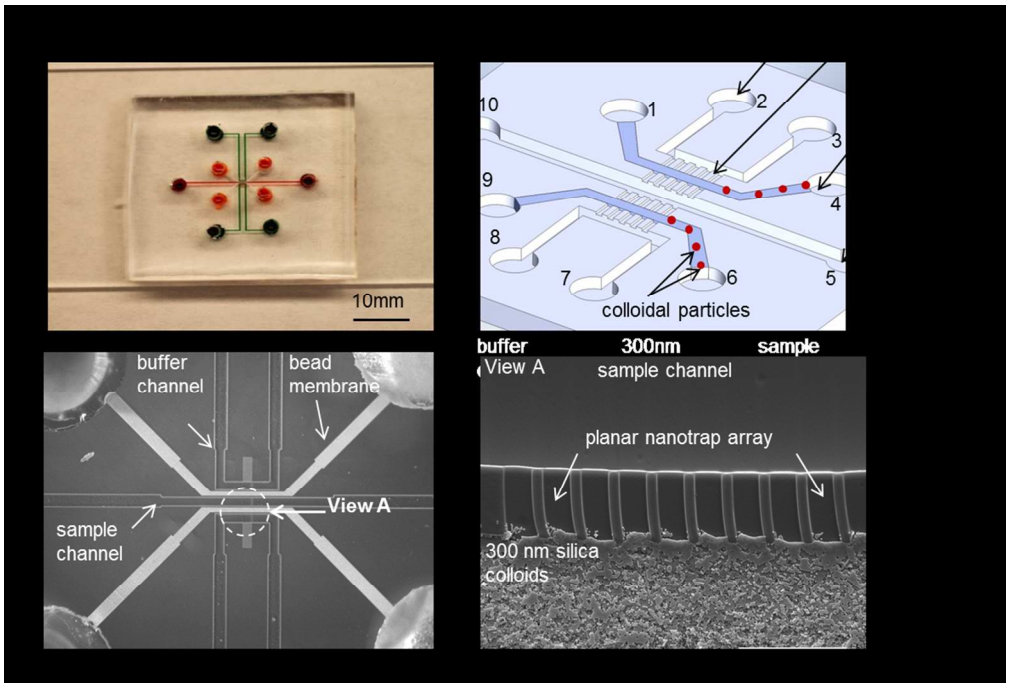

199x135mm (150 x 150 DPI)

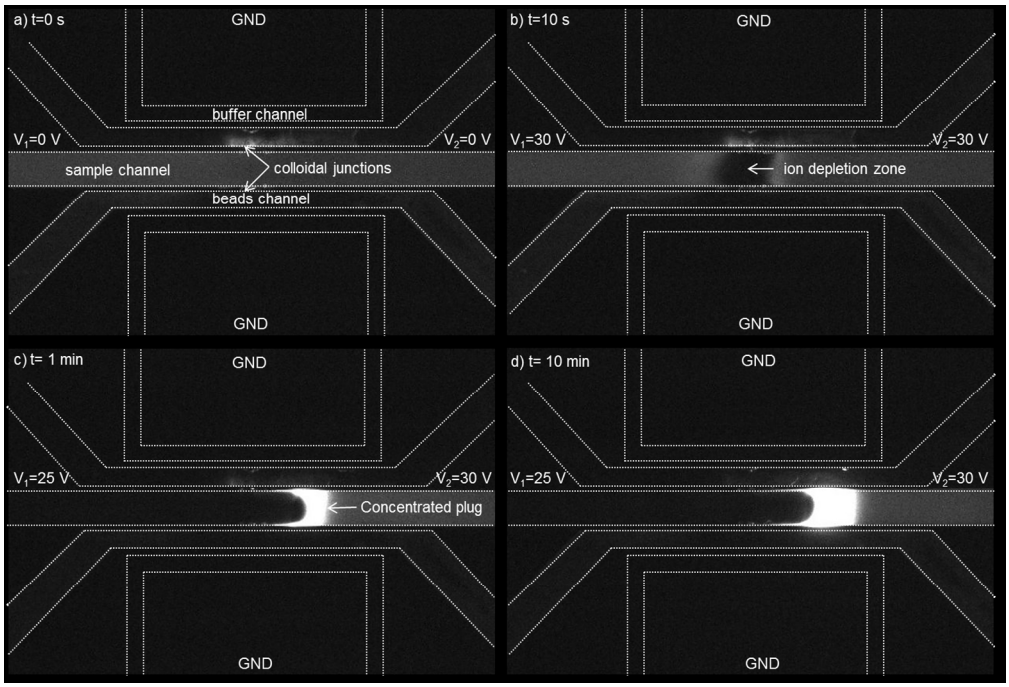

256x173mm (150 x 150 DPI)

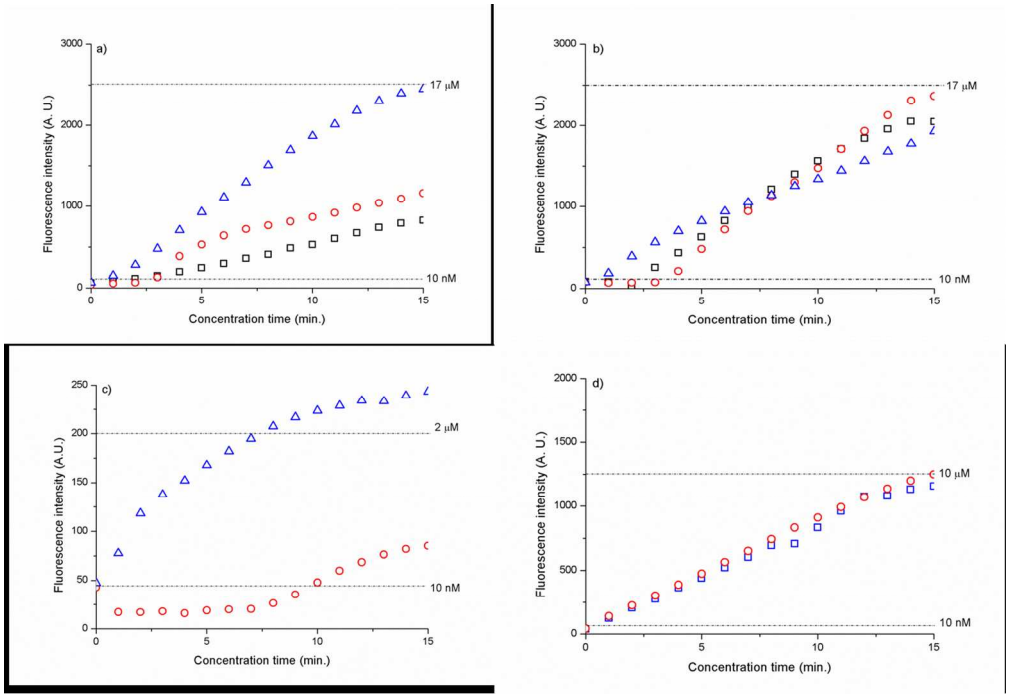

255x175mm (150 x 150 DPI)